Optical bistability from three-level atoms with the use of a coherent nonlinear mechanism

J. Mlynek, F. Mitschke, R. Deserno, and W. Lange
Institut für Quantenoptik, Universität Hannover, Welfengarten 1, D-3000 Hannover 1, Federal Republic of Germany
(Received 18 April 1983)

We report on studies on optical bistability from coherently driven Λ-type three-level atoms in a Fabry-Perot resonator. The nonlinear mechanism relies on transverse optical pumping and is due to population trapping in a coherent superposition of the ground-state sublevels. If, under appropriate conditions, a zero-field level-crossing resonance (Hanle resonance) occurs in the atomic system, the optical device is shown to display dispersive or absorptive bistability. Our theoretical studies are based on numerical solutions of the corresponding three-level Bloch equations in the presence of optical feedback. Experiments are performed on the D_1 line in a sodium-filled Fabry-Perot resonator using transverse optical Zeeman pumping of the $^2S_{1/2}$ ground state. The measurements are found to be in fair agreement with the theoretical predictions from our simple model.

I. INTRODUCTION

Optical bistability (OB) using depopulation pumping is a well-known scheme. In 1976, Gibbs, McCall, and Venkatesan[1] experimentally demonstrated that a Fabry-Perot cavity filled with sodium vapor as a nonlinear medium exhibits optical bistability. They used nonlinear dispersion due to hyperfine pumping in the ground state. More recently, longitudinal Zeeman pumping in the Na ground state has been demonstrated as a mechanism for low-threshold OB.[2] In fact, these pumping schemes generally do not require atomic saturation: They take advantage of population storage in an optically decoupled ground-state sublevel to reduce the effective saturation intensity of the driven transition. Thus, bistability may occur at largely reduced thresholds as compared to two-level systems.[2,3]

A reduced switching threshold is also expected for OB using transverse optical pumping.[4] However, in this latter pumping scheme, the nonlinear mechanism is different: it relies on two-photon induced *sublevel coherence* effects. If, under appropriate conditions, a Hanle-type resonance[5] occurs in this system [see Fig. 1(b)], the atoms are efficiently accumulated in a coherent superposition of (degenerate) Zeeman sublevels; this Zeeman coherence turns out to be decoupled from the excited state and the induced polarization strongly decreases in zero magnetic field. In the presence of optical feedback the nonlinearity of this zero-field level-crossing resonance can then give rise to dispersive or absorptive optical bistability and hysteresis. Moreover, due to the Raman-type transition, the nonlinear mechanism is supposed to be relatively insensitive to Doppler and laser-bandwidth effects.[4]

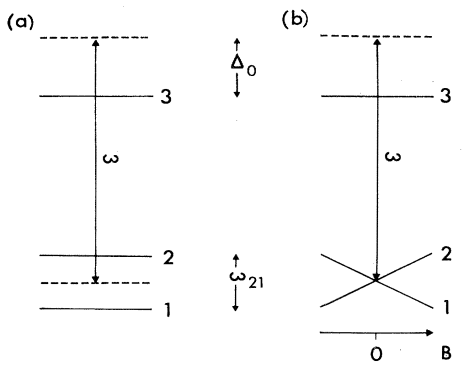

FIG. 1. (a) Λ-type three-level system, (b) ground-state level crossing in a magnetic field B.

Recently, we reported a preliminary account of optical bistability utilizing transverse optical Zeeman pumping as a nonlinear mechanism.[6] In this paper a more detailed discussion of the experiment and its underlying theory will be presented. Our theoretical studies are based on numerical solutions of the corresponding three-level Bloch equations in the presence of optical feedback (Sec. II). Experiments were performed on the D_1 line in a sodium-filled Fabry-Perot resonator using optically induced ground-state Zeeman coherence (Sec. III). The comparison of measurements and numerical studies eventually allows us to test our simple theoretical model (Sec. IV).

II. PHYSICAL MODEL

A. Nonlinear medium

Consider a folded Λ-type three-level system interacting with a single-mode radiation field of frequency ω [Fig. 1(a)]. We assume Zeeman sublevels that can be tuned by means of a magnetic field B [Fig. 1(b)]; $\omega_{21}/2\pi$ then denotes the Larmor frequency of the system. Our analysis is based on the density-matrix formalism. The corresponding Bloch equations for the radiatively coupled three-level atom are well known and can be found elsewhere.[7,8] Here we will restrict ourselves to a quick outline of the basic assumptions underlying our calculations and to the discussion of the relevant results.

With the use of the Bloch equations the polarization P and the susceptibility χ of the medium can be determined. To simplify the problem, we completely neglect the tensorial character of the susceptibility, i.e., we treat the problem as a scalar one. The knowledge of χ then easily

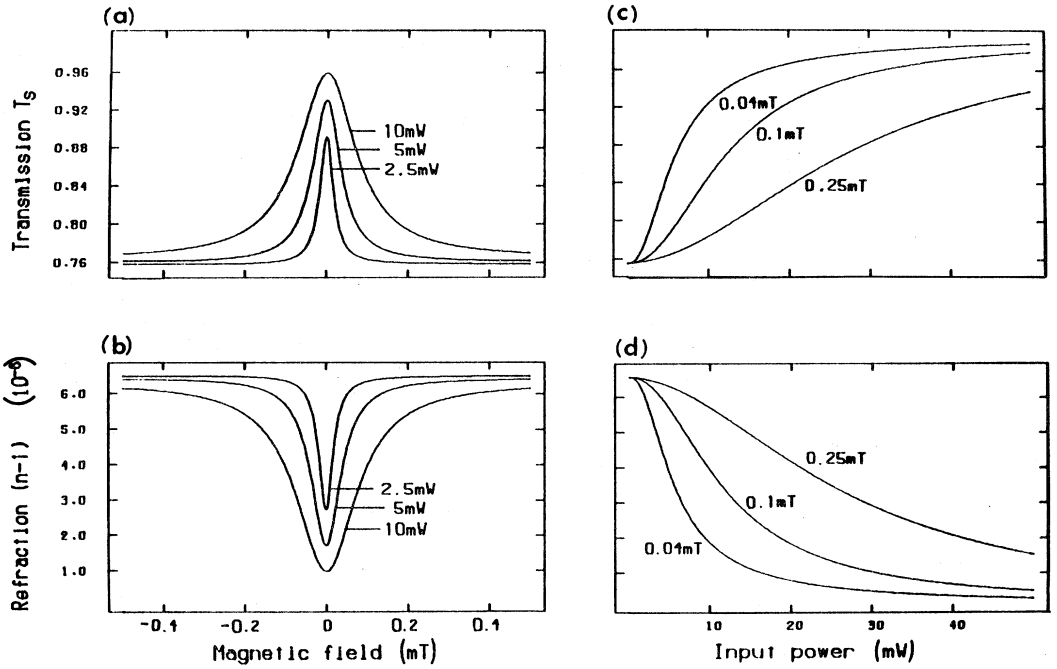

FIG. 2. (a) and (b) Calculated sample transmission T_S and index of refraction $n-1$ as a function of the external magnetic field B for the three-level medium; the parameter is the input power (beam diameter, 240 μm). (c) and (d) Calculated variations of T_S and $n-1$ with input power for three different magnetic field values. The other parameter values are $N=1.08\times10^{13}$ cm^{-3}, $l=2$ cm, argon buffer-gas pressure $p_{AR}=131$ mbar, $d=240$ μm, dipole matrix element $\mu=8.5\times10^{-30}$ Cm, $T_1=16$ nsec, $T_2=0.16$ nsec, $\tau_1=\tau_2=6.7$ μsec, $\omega_{21}/2\pi=B(14$ MHz/mT), $\Delta_0/2\pi=-10$ GHz.

allows us to determine the index of refraction n and the absorption coefficient α of our medium. We solved the problem numerically using the following notations for the atomic system: T_1 is the lifetime of level 3 and T_2 describes the relaxation time of the optical coherences. Correspondingly, τ_1 denotes the nonradiative longitudinal relaxation time between sublevels 1 and 2 and τ_2 is the nonradiative dephasing time of the sublevel coherence. Let us mention that for optically pumped ground-state sublevels of an atomic vapor, τ_1 and τ_2 are generally rather large.[9]

In Figs. 2(a) and 2(b) the sample transmission $T_S=\exp(-2\alpha l)$ and $n-1$ are shown as a function of the magnetic field B, i.e., of the sublevel splitting ω_{21}, for off-resonant excitation ($\Delta_0/2\pi=-10$ GHz) and different input powers. Throughout this paper we assume a beam diameter of 240 μm and use light powers instead of intensities for the ease of comparison with experiments. The variations of T_S and $n-1$ with input power for various magnetic field values B and the same Δ_0 are plotted in Figs. 2(c) and 2(d). The complete set of parameter values is given in the figure caption; they are much like the values used in our experiment. In calculating T_S and n we have neglected propagation effects, i.e., α and n are assumed to be constant over the sample length l. T_S and n obviously display narrow resonance structures when ω_{21} is scanned through zero. This is due to the mechanism of coherent population trapping that also gives rise to a nonabsorption resonance in the population of the excited state.[8,10] Let us mention that the signal shown in Fig. 2(a) has also been called "level crossing in stimulated emission";[5] generally its width in frequency units can be much narrower than the corresponding optical linewidth. For example, the narrowest resonance in Fig. 2(a) has a width (FWHM) of about 500 kHz which is small compared to the assumed optical linewidth of $1/\pi T_2=2$ GHz. As can also be seen from Fig. 2, near level crossing, T_s and n show a pronounced dependence on input intensity and on magnetic field B. For $\Delta_0=0$, it turns out that no resonance occurs for n and the system behaves purely absorptive. In the limit $\tau_1,\tau_2\rightarrow\infty$, this latter situation has been discussed analytically in Ref. 4.

B. Nonlinear Fabry-Perot resonator

The nonlinearity of this sublevel resonance can give rise to optical bistability if the medium is subjected to optical feedback, e.g., by being placed into an optical resonator. To further simplify the problem, we assume the three-level medium to be located within a Fabry-Perot cavity and we neglect Doppler broadening, transverse intensity variations, standing-wave effects, and propagation effects as mentioned above. The intracavity intensity I_c is found to be given by a somewhat generalized Airy formula:

$$\frac{I_c}{I_{\text{in}}}=\frac{T_M T_S T_R}{(1-R_M T_S T_R)^2}\frac{1}{1+F\sin^2[\frac{1}{2}(\delta_s+\delta_0)]}, \tag{1}$$

$$F=4R_M T_S T_R/(1-R_M T_S T_R)^2, \tag{2}$$

$$\delta_s=4\pi(n-1)l/\lambda, \tag{3}$$

$$\delta_0 = 4\pi L/\lambda + \delta_R \ . \tag{4}$$

Here R_M and T_M are the mirror reflectivity and the mirror transmissivity, respectively. T_S describes the sample transmission and δ_S is the phase shift due to the sample dispersion. δ_0 denotes the empty-cavity phase shift with L being the cavity length. T_R and δ_R are parameters to formally describe additional residual intracavity losses and phase shifts, respectively. T_S and n characterize the nonlinear medium and, with respect to our three-level system, depend, e.g., on sublevel splitting ω_{21} and on intracavity intensity I_c. Consequently, Eq. (1) is transcendent in I_c and generally can only be solved numerically. Thus, for a given I_{in}, the corresponding I_c is found if T_S and n, as calculated from the Bloch equations, also satisfy the resonator equation (1).

In Figs. 3 and 4 the predicted output power $P_T = T_M P_c$ of a Fabry-Perot resonator filled with the three-level medium is shown as a function of the magnetic field for different situations. For $\Delta_0 = 0$ dispersion is zero and the system behaves purely absorptive; this case corresponds to Fig. 3 where P_T is plotted for two input powers. The inserted arrows indicate the hysteresis cycle that occurs by scanning the B field forth and back through zero. For large optical detunings Δ_0 the device is dominated by dispersive effects and the form of the bistability curve changes characteristically. This can be seen in Fig. 4 for $\Delta_0/2\pi = -10$ GHz and two different empty-cavity mistunings. The detailed parameter values corresponding to Figs. 3 and 4 are all listed in the figure captions.

III. MEASUREMENTS

A. Experimental setup

A schematic diagram of the apparatus for the bistability experiment is shown in Fig. 5. Experiments were performed on the Na D_1 line using a home-built single-mode cw dye laser with a maximum output power of 300 mW. No active laser stabilization techniques were used and the laser linewidth in the free-running mode was estimated to be $\lesssim 20$ MHz at 598.6 nm. A Faraday rotator was used to optically isolate the laser from the bistable device. After being circularly polarized by a $\lambda/4$ plate the laser beam was then focused into a Fabry-Perot resonator (FP) containing the sodium sample. The FP was nearly confocal (mirror curvature, 15 cm), and the focusing lens (focal length, 15 cm) served for mode-matching purposes. The resulting intracavity beam diameter was calculated to be 240 μm. For a variation of cavity length one mirror was mounted on a piezoelectric translator (PZT) drive. Mirror reflectivities of $R_M = 0.9$ were used and the finesse of the FP with the cold Na cell placed inside was measured as 10 (free spectral range, 1 GHz).

The sodium vapor is contained in a heated stainless-steel cell of 1 cm diameter, the length of the heated zone being 2 cm. Typical Na number densities used in the experiments were 10^{13} cm^{-3} with about 200 mbar argon buffer gas added. The sodium cell was mounted in a water-cooled housing that was thermalized to room temperature to minimize thermal gradients within the cavity. The cell windows were slightly tilted with respect to each other and antireflection coated on both surfaces to prevent spurious optical feedback within the FP.

The Ar buffer gas not only prevented a contamination of the cell windows but also served several additional purposes. At the high pressures used ($p_{\text{Ar}} \cong 200$ mbar) the

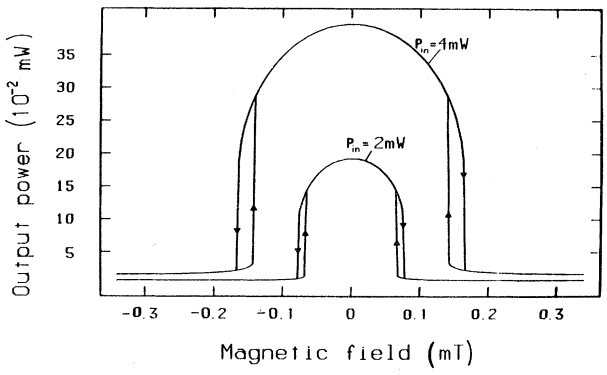

FIG. 3. Absorptive case $\Delta_0 = 0$, calculated cavity output as a function of the external magnetic field B for two different input powers. The medium is characterized by $N = 5.3 \times 10^{11}$ cm^{-3}, $p_{\text{Ar}} = 131$ mbar, $\mu = 8.5 \times 10^{-30}$ Cm, $T_1 = 16$ nsec, $T_2 = 0.16$ nsec, $\omega_{21}/2\pi = B(7$ MHz/mT), $\tau_1 = \tau_2 = 8.2$ μsec. The cavity parameter values are $L = 15$ cm, $R_M = 0.9$, $T_R = 0.8$, $\delta_0 = 0$.

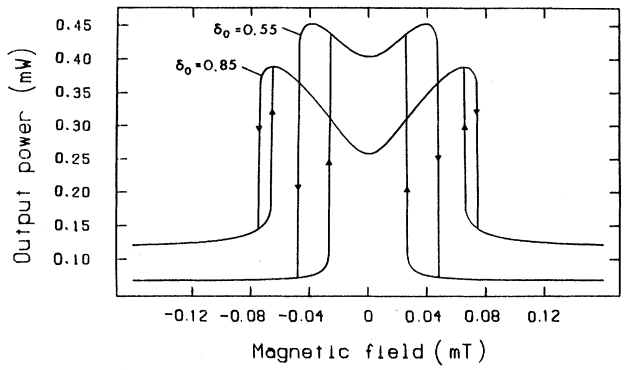

FIG. 4. Dispersive case $\Delta_0/2\pi = 10$ GHz; calculated cavity output as a function of the external magnetic field for two different empty cavity phase shifts δ_0 ($\delta_0 = 0.55 \leftrightarrow 87.5$ MHz empty cavity mistuning, $\delta_0 = 0.85 \leftrightarrow 135$ MHz). Parameter values are $N = 5.6 \times 10^{12}$ cm^{-3}, $P_{\text{in}} = 6$ mW, otherwise as in Fig. 3.

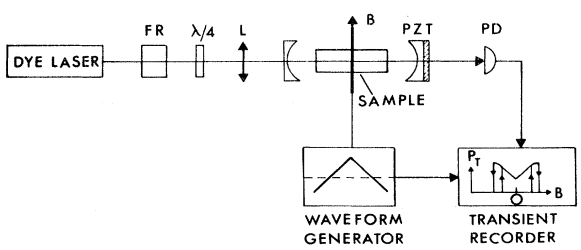

FIG. 5. Schematic of the experimental arrangement: FR, Faraday rotator; $\lambda/4$, retardation plate; L, mode-matching lens; PZT, piezoelectric translator; PD, photodiode; B, transverse magnetic field.

collisional broadening of the D_1 line was $\Delta\nu_p \cong 3$ GHz (Ref. 11) and thus masks the ground-state hyperfine structure (1.8 GHz) as well as the Doppler distribution ($\Delta\nu_D \cong 2$ GHz). Thus, we expect the line to be essentially homogeneously broadened. Moreover, the collisions with buffer gas rapidly mix the upper-state sublevels, and the excited-state manifold can thus be approximated as one level. On the other hand, the ground-state sublevels are practically unaffected by buffer-gas collisions. In addition, diffusion times of optically pumped atoms out of the laser beam become longer in the presence of high buffer-gas pressure. Finally, the collisions are important for the efficient creation of Zeeman coherence under conditions of off-resonant optical excitation.[12] Let us note that under the experimental conditions reported here, the ground-state relaxation times were mainly diffusion limited ($\tau_1 \cong \tau_2$) and were found to be about 7 μsec.[13]

A pair of Helmholtz coils was used to create a small transverse magnetic field B up to a strength of a few 0.1 mT. Two additional pairs of coils were used to compensate for the Earth's magnetic field. Owing to the residual magnetization of the metallic cell, however, this compensation was not complete; the remaining field was about 0.01 mT. A waveform generator was used to control the electric current flowing through the Helmholtz coils; this allowed us to continuously sweep the transverse B field forth and back through zero. The corresponding sweep rate was set low enough ($\lesssim 10$ Hz) to avoid signal distortions due to transient effects. On the other hand, the sweep time was set fast enough (> 0.1 Hz) to prevent the signal from being influenced by a cavity drift due to changes in pressure or temperature of the surrounding air.

In a transverse magnetic field B the circularly polarized light beam coherently couples adjacent Zeeman sublevels ($|\Delta m_F| = 1$, $F = 1,2$) of the $^2S_{1/2}$ ground state via the excited $^2P_{1/2}$ state. Neglecting nuclear magnetism, the g_F factors for the two ground-state hyperfine levels only differ by sign ($|g_F| = 0.5$) and in a weak field B the Larmor frequency is given by B(7 MHz)/mT for both F states. This variable splitting frequency corresponds to $\omega_{21}/2\pi$ in Fig. 1. It should be noted, however, that atomic sodium does not represent a single three-level system but is composed of a manifold of coupled three-level systems. Therefore, Fig. 1 is only a crude model for our atomic medium.

The laser light being transmitted through the FP was monitored by a photodiode and the signal was then stored in a transient recorder (Datalab DL 922). It was operated in the x-y mode with its x deflection being controlled by the voltage ramp of the waveform generator. Consequently, the FP output power P_T could directly be monitored as a function of the transverse B field. The single-sweep signals were sent to a minicomputer for storage and further analysis.

Let us note that we also performed experiments where the input laser power was varied instead of the B field. For this purpose an electro-optic modulator (EOM) was introduced in between the Faraday rotator (FR) and $\lambda/4$ plate. By applying an appropriate voltage ramp to the EOM, the input power P_{in} could then be scanned. P_{in} was monitored in addition to P_T by using a second photodiode

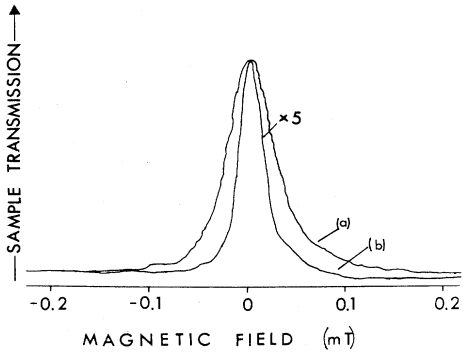

FIG. 6. Measured optical transmission of Na vapor as a function of transverse magnetic field for two input intensities (a) $I_0 = 30$ W/cm^2 and (b) $0.6I_0$.

and the ratio P_T/P_{in} was determined by means of an analog divider. Its value that is proportional to the cavity transmission was then recorded as a function of the input power P_{in} with the use of the transient recorder.

B. Experimental results

In order to demonstrate the occurrence of a nonabsorption resonance under conditions of transverse optical Zeeman pumping, we first performed a simple transmission experiment without cavity feedback, i.e., by misaligning the resonator. In Fig. 6 a typical result is shown for the sample transmission as a function of the transverse magnetic field B for two different input intensities. Here the laser was tuned close to the center of the D_1 line. The sodium vapor density corresponded to an optically thick sample: at higher magnetic field values ($B > 0.2$ mT) the sample absorption was about 95%. When the ground-state Zeeman splitting was scanned through degeneracy, a narrow transmission peak showed up. As can be seen from Fig. 6 its width $\Delta\nu = (7\text{ MHz})\Delta B/\text{mT}$ (full width at half maximum) is less than 1 MHz; this value is small compared to the pressure-broadened optical linewidth that

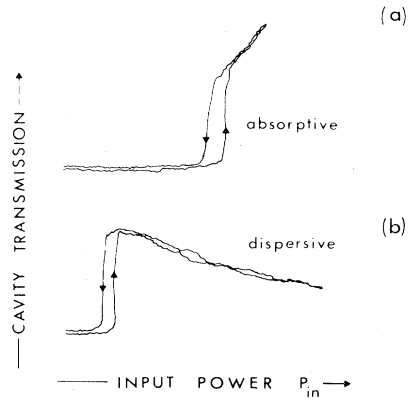

FIG. 7. Typical curves of the observed cavity transmission as a function of input power under (a) absorptive and (b) dispersive conditions.

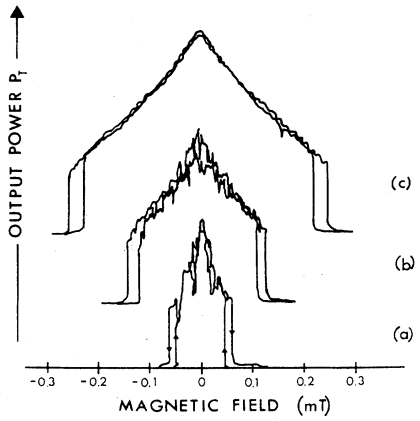

FIG. 8. Measured cavity output power in the absorptive regime as a function of the transverse magnetic field B for three different number densities: (a) $N_{Na} \cong 1.9 \times 10^{12}$ cm^{-3}, (b) $N_{Na} \cong 2.4 \times 10^{12}$ cm^{-3}, (c) $N_{Na} \cong 3.9 \times 10^{12}$ cm^{-3}. Otherwise $p_{Ar} = 120$ mbar, $P_{in} = 150$ mW, zero cavity mistuning; for other parameter values see text. Arrows indicate the observed hysteresis cycle.

was about 2 GHz corresponding to a buffer-gas pressure of 130 mbar. Similar Hanle-type resonances were also observed for off-resonant excitation with laser detunings $\Delta_0/2\pi$ up to 30 GHz. These measurements demonstrate that under appropriate conditions, the sample transmission is strongly dependent on incident laser intensity and on the Zeeman sublevel splitting.

With optical feedback, the nonlinearity of the medium gave rise to optical bistability. In Fig. 7 typical experimental results are shown for the cavity transmission as a function of input intensity for the absorptive and the dispersive case in zero external B field. Optical bistability dominated by absorption is more difficult to realize since it only occurs for a particular detuning of the laser within the absorption profile of the D_1 line. This indicates a region of negligible nonlinear refraction where n is not altered by optical pumping.[1] For the same laser detuning we also observed symmetric Airy peaks in the cavity transmission as a function of cavity mistuning; otherwise, these peaks were observed always to be asymmetric, indicating dispersive contributions. Let us emphasize with respect to Fig. 7(a) that the transmission grows monotonically in the upper branch as expected for absorptive systems.[14]

Figure 8 shows the output intensity as a function of the external magnetic field for various number densities with

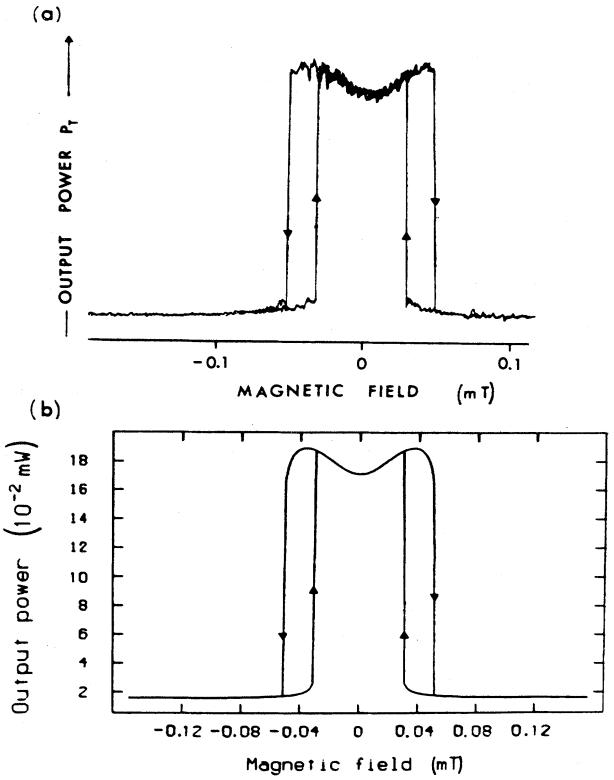

FIG. 10. Measured (a) and calculated (b) dispersive bistability and hysteresis for $\Delta_0/2\pi = 3.5$ GHz. Parameter values are (a) $N_{Na} \cong 5 \times 10^{12}$ cm^{-3}, $p_{Ar} = 200$ mbar, $P_{in} = 80$ mW, $d = 240$ μm, cavity mistuning not experimentally determined. (b) $N = 2.7 \times 10^{12}$ cm^{-3}, $p_{Ar} = 200$ mbar, $P_{in} = 3.7$ mW, $d = 240$ μm, $\mu = 8.5 \times 10^{-30}$ Cm, $T_1 = 16$ nsec, $T_2 = 0.11$ nsec, $\tau_1 = \tau_2 = 11.3$ μsec, $l = 2$ cm, $L = 15$ cm, $R_M = 0.9$, $T_R = 0.8$, $\delta_0 = 0.41$.

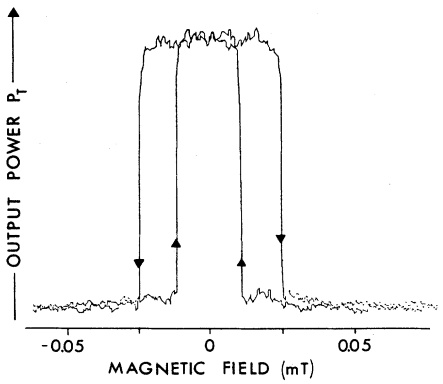

FIG. 9. Dispersive bistability for $\Delta_0/2\pi = 8$ GHz. Parameter values are $N_{Na} \cong 3 \times 10^{12}$ cm^{-3}, $p_{Ar} = 200$ mbar, $P_{in} = 60$ mW, cavity mistuning not experimentally determined.

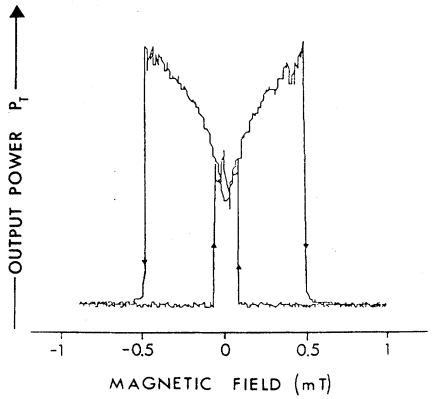

FIG. 11. Dispersive bistability for $\Delta_0/2\pi = 10$ GHz. Parameter values are $N_{Na} \cong 8 \times 10^{12}$ cm^{-3}, $p_{Ar} = 215$ mbar, $P_{in} = 80$ mW, cavity mistuning not experimentally determined.

the laser detuning as just explained, i.e., under mainly absorptive conditions. As predicted, optical bistability and hysteresis are observed when the Zeeman sublevels are scanned forth and back through level degeneracy. Absorptive optical bistability could only be observed at high laser powers ($P_{in} > 50$ mW) and over a small range of sodium number densities ($10^{12} - 10^{13}$ cm^{-3}). Moreover, as pointed out above, the laser frequency stability was crucial in these measurements.

Most experiments were performed in the dispersive regime: some representative results are shown in Figs. 9, 10(a), and 11. These curves demonstrate that, depending on experimental conditions, various signal forms can be obtained; also note in this respect that different scales in B field are used in these figures. Dispersive optical bistability could be realized over a wide range of parameter values; it was obtained, e.g., for laser detunings up to 40 GHz. As expected, the signal shapes were also strongly dependent on the cavity mistuning that could be varied by means of the PZT. Owing to a lack in stability of the Fabry-Perot resonator, however, it was not possible either to determine accurately this parameter value nor to study its influence in detail. For further experiments we are thus planning to stabilize the cavity length by means of a He-Ne laser. Variations of the buffer-gas pressure over the range 25—250 mbar did not significantly affect the overall signal shape. With increasing laser power, the bistable switching occurred at increasingly higher magnetic field values; at the same time the hysteresis got broader. No bistable switching could be obtained for input powers below 10 mW.

IV. DISCUSSION

The experimental results shown in Figs. 8—11 have to be compared to our calculated curves (see Figs. 3 and 4). In the absorptive case the measured and the calculated signals both display a roof-type structure in between the switching points. The measured curves, however, always showed a nearly triangular shape, whereas the calculated absorptive curves (Fig. 3) are completely rounded off; the origin of this difference is not yet known. It might have various reasons: as mentioned above our model neglects the Gaussian cavity mode, propagation effects, standing-wave effects, and the Doppler effect. Calculations including Doppler integration have not given any evidence for a significant change in the shape of the absorptive curve as compared to Fig. 3; this reflects the fact that our medium is mainly pressure broadened. Standing-wave effects were ruled out by repeating the experiment in a ring cavity; the signal form was observed to be essentially the same as in the Fabry-Perot experiment. Thus, the measured signal shape might be affected by the Gaussian transverse intensity distribution and/or by propagation effects in our cavity; so far, these effects have not been examined in detail. It should be mentioned, however, that first numerical studies taking into account the intensity variations over the beam profile yield better agreement with the experimentally observed absorptive signal shapes.

Good qualitative agreement between theory and experiment is obtained for the dispersive case: Figure 10(b), e.g., shows a calculated curve for parameter values that nearly fit those of the measured curve [Fig. 10(a)]. They essentially differ in input intensity; we found out that the experimentally used intensities generally are larger by about 1 order of magnitude than the calculated ones under otherwise comparable experimental conditions. The same discrepancy is found in a quantitative comparison of measured and calculated data for the absorptive case. This quantitative disagreement in intensity dependence is not surprising due to the simplicity of our model. As an example given, we assume a single three-level system, whereas the Na level scheme is much more complicated; this necessarily modifies the intensity requirements for switching. On the other hand, our simple model seems to reflect the basic physical features of the device quite reasonably.

It should be noted that very recently new features like polarization switching[15] and self-oscillations induced by a transverse magnetic field[16] have been observed in experiments on optical resonators filled with sodium atoms. In these experiments, however, the light was linearly polarized and the analysis is based on a decomposition of the light field into right- and left-circularly polarized components, while circularly polarized light was used in the present experiment. Interestingly enough, the occurrence of self-oscillations in Na vapor induced by a transverse magnetic field cannot generally be excluded in the case of circularly polarized input light; further analysis, however, shows that it is not to be expected under the experimental conditions used here.

V. CONCLUSION

In conclusion, our experiments show that sublevel coherence effects can be used as an efficient mechanism in bistability experiments. For the case of Zeeman sublevels we have demonstrated the use of a static magnetic field in a bistable system. Experimentally, an external magnetic field is easily variable and might prove useful as a control parameter in other types of nonlinear optical devices. Very recently, e.g., multistabilities in intracavity phase conjugation through degenerate four-wave mixing have been observed by use of Zeeman coherence effects.[17] Thus, ground-state atoms with Zeeman sublevels being subjected to transverse optical pumping in an optical feedback loop seem to display a manifold of interesting nonlinear phenomena.

ACKNOWLEDGMENT

This work was supported by the Deutsche Forschungsgemeinschaft.

[1]H. M. Gibbs, S. L. McCall, and T. N. C. Venkatesan, Phys. Rev. Lett. 36, 1135 (1976).
[2]F. T. Arecchi, G. Giusfredi, E. Petriella, and P. Salieri, Appl. Phys. B 29, 79 (1982).
[3]R. J. Ballagh, J. Cooper, and W. J. Sandle, J. Phys. B 14, 3881 (1981).
[4]D. F. Walls and P. Zoller, Opt. Commun. 34, 260 (1980).
[5]See, e.g., M. S. Feld, A. Sanchez, A. Javan, and B. J. Feldman, in *Proceedings of the Aussois Conferences on High-Resolution Molecular Spectroscopy* (Colloques Internationaux de CNRS, Paris, 1973), pp. 87–104.
[6]J. Mlynek, F. Mitschke, R. Deserno, and W. Lange, Appl. Phys. B 28, 135 (1982).
[7]R. G Brewer and E. L. Hahn, Phys. Rev. A 11, 1641 (1975).
[8]G. Orriols, Nuovo Cimento B 53, 1 (1979).
[9]See, e.g., W. Happer, Rev. Mod. Phys. 44, 169 (1972).
[10]H. R. Gray, R. M. Whitley, and C. R. Stroud, Jr., Opt. Lett. 3, 218 (1978).
[11]R. H. Chatham, A. Gallagher, and E. L. Lewis, J. Phys. B 13, L7 (1980).
[12]N. Bloembergen, A. R. Bogdan, and M. W. Downer, in *Laser Spectroscopy V,* edited by A. R. W. McKellar, R. Oka, and B. P. Stoicheff (Springer, Heidelberg, 1981), p. 157.
[13]F. Mitschke, R. Deserno, J. Mlynek, and W. Lange, Opt. Commun. 46, 135 (1983).
[14]J. D. Cresser and P. Meystre, in *Optical Bistability,* edited by C. M. Bowden, M. Ciftan, and H. R. Robl (Plenum, New York, 1981), pp. 265–279.
[15]S. Cecchi, G. Giusfredi, E. Petriella, and P. Salieri, Phys. Rev. Lett. 49, 1928 (1982), and references therein.
[16]F. Mitschke, J. Mlynek, and W. Lange, Phys. Rev. Lett. 50, 1660 (1983), and references therein.
[17]J. Mlynek, F. Mitschke, E. Köster, and W. Lange, in *Coherence and Quantum Optics V,* edited by L. Mandel and E. Wolf (Plenum, New York, in press).